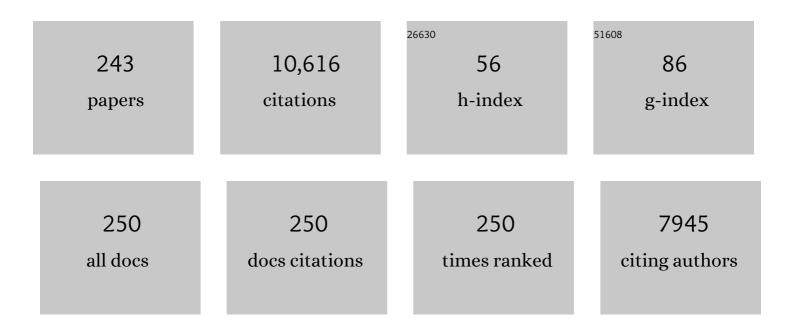
List of Publications by Year in descending order

Source: https://exaly.com/author-pdf/3576127/publications.pdf Version: 2024-02-01



Ινιςλείμμο

#	Article	IF	CITATIONS
1	Strengthening absorption ability of Co–N–C as efficient bifunctional oxygen catalyst by modulating the d band center using MoC. Green Energy and Environment, 2023, 8, 459-469.	8.7	22
2	Directionally maximizing CO selectivity to near-unity over cupric oxide with indium species for electrochemical CO2 reduction. Chemical Engineering Journal, 2022, 427, 131654.	12.7	18
3	Hydrogen generation and utilization in a two-phase flow membraneless microfluidic electrolyzer-fuel cell tandem operation for micropower application. Applied Energy, 2022, 305, 117945.	10.1	13
4	Constructing novel cross-linked polybenzimidazole network for high-performance high-temperature proton exchange membrane. Journal of Membrane Science, 2022, 643, 120037.	8.2	60
5	ZnS anchored on porous N, S-codoped carbon as superior oxygen reduction reaction electrocatalysts for Al-air batteries. Journal of Colloid and Interface Science, 2022, 609, 868-877.	9.4	6
6	Interfaceâ€Induced Electrocatalytic Enhancement of CO ₂ â€ŧoâ€Formate Conversion on Heterostructured Bismuthâ€Based Catalysts. Small, 2022, 18, e2105682.	10.0	53
7	Tuning the subsurface oxygen of Ag2O-derived Ag nanoparticles to achieve efficient CO2 electroreduction to CO. Electrochimica Acta, 2022, 403, 139656.	5.2	4
8	In-situ generated hydroxides realize near-unity CO selectivity for electrochemical CO2 reduction. Chemical Engineering Journal, 2022, 433, 133785.	12.7	9
9	Lessâ€Energy Consumed Hydrogen Evolution Coupled with Electrocatalytic Removal of Ethanolamine Pollutant in Saline Water over Ni@Ni ₃ S ₂ /CNT Nanoâ€Heterostructured Electrocatalysts. Small Methods, 2022, 6, e2101195.	8.6	10
10	<i>In situ</i> construction of hetero-structured perovskite composites with exsolved Fe and Cu metallic nanoparticles as efficient CO ₂ reduction electrocatalysts for high performance solid oxide electrolysis cells. Journal of Materials Chemistry A, 2022, 10, 2509-2518.	10.3	30
11	Bariumâ€doped Sr ₂ Fe _{1.5} Mo _{0.5} O _{6â€} <i>_δ</i> perovskite anode materials for protonic ceramic fuel cells for ethane conversion. Journal of the American Ceramic Society, 2022, 105, 3613-3624.	3.8	9
12	Toward Excellence of Electrocatalyst Design by Emerging Descriptorâ€Oriented Machine Learning. Advanced Functional Materials, 2022, 32, .	14.9	43
13	Electrochemically reconstructed perovskite with cooperative catalytic sites for CO2-to-formate conversion. Applied Catalysis B: Environmental, 2022, 306, 121101.	20.2	14
14	Influence of Major Operating Parameters (Temperature, Pressure, and Flow Rate) on the Corrosion of Candidate Alloys for the Construction of Hydrothermal Liquefaction Biorefining Reactors. Energy & Fuels, 2022, 36, 3134-3153.	5.1	5
15	Lessâ€Energy Consumed Hydrogen Evolution Coupled with Electrocatalytic Removal of Ethanolamine Pollutant in Saline Water over Ni@Ni ₃ S ₂ /CNT Nanoâ€Heterostructured Electrocatalysts (Small Methods 3/2022). Small Methods, 2022, 6, .	8.6	1
16	NiFe P@NiCo-LDH nanoarray bifunctional electrocatalysts for coupling of methanol oxidation and hydrogen production. International Journal of Hydrogen Energy, 2022, 47, 17150-17160.	7.1	21
17	Densely packed ultrafine SnO2 nanoparticles grown on carbon cloth for selective CO2 reduction to formate. Journal of Energy Chemistry, 2022, 71, 159-166.	12.9	17
18	Generation of hydrogen accompanied with formate bifunctional NiCo P@NiCo-LDH nanosheet electrocatalyst. Journal of Alloys and Compounds, 2022, 906, 164305.	5.5	6

#	Article	IF	CITATIONS
19	Regulating the Electron Localization of Metallic Bismuth for Boosting CO2 Electroreduction. Nano-Micro Letters, 2022, 14, 38.	27.0	21
20	Nanoalloy libraries from laser-induced thermionic emission reduction. Science Advances, 2022, 8, eabm6541.	10.3	11
21	Carbon Dioxide Valorization via Formate Electrosynthesis in a Wide Potential Window. Advanced Functional Materials, 2022, 32, .	14.9	37
22	Impacts of catalyst, inorganic and organic corrodants on corrosion under batch-mode catalytic biomass hydrothermal liquefaction conversion. Corrosion Science, 2022, 204, 110409.	6.6	6
23	High ionic conductivity of ultralow yttria concentration yttria-stabilized zirconia thin films. Journal of Vacuum Science and Technology A: Vacuum, Surfaces and Films, 2022, 40, 042405.	2.1	2
24	Switchable CO ₂ Electroreduction Induced By the Bismuth Moiety with Tunable Local Structures on Graphene. ECS Meeting Abstracts, 2022, MA2022-01, 2090-2090.	0.0	0
25	Tailoring a Three-Phase Microenvironment for High-Performance CO ₂ Electroreduction. ECS Meeting Abstracts, 2022, MA2022-01, 1770-1770.	0.0	0
26	Interface modification of Ru-CeO2 co-infiltrated SFM electrode and construction of SDC/YSZ bilayer electrolyte for direct CO2 electrolysis. Electrochimica Acta, 2022, 426, 140771.	5.2	9
27	Efficient bifunctional electrocatalysts for solid oxide cells based on the structural evolution of perovskites with abundant defects and exsolved CoFe nanoparticles. Journal of Power Sources, 2021, 482, 228981.	7.8	36
28	In situ facile fabrication of Ni(OH)2 nanosheet arrays for electrocatalytic co-production of formate and hydrogen from methanol in alkaline solution. Applied Catalysis B: Environmental, 2021, 281, 119510.	20.2	154
29	Hollow NiSe Nanocrystals Heterogenized with Carbon Nanotubes for Efficient Electrocatalytic Methanol Upgrading to Boost Hydrogen Coâ€Production. Advanced Functional Materials, 2021, 31, 2008812.	14.9	84
30	All roads lead to Rome: An energy-saving integrated electrocatalytic CO2 reduction system for concurrent value-added formate production. Chemical Engineering Journal, 2021, 412, 127893.	12.7	38
31	Ultrasmall Bi nanoparticles confined in carbon nanosheets as highly active and durable catalysts for CO2 electroreduction. Applied Catalysis B: Environmental, 2021, 284, 119723.	20.2	61
32	Interfacial engineering of Cu2Se/Co3Se4 multivalent hetero-nanocrystals for energy-efficient electrocatalytic co-generation of value-added chemicals and hydrogen. Applied Catalysis B: Environmental, 2021, 285, 119800.	20.2	51
33	Reducing d-p band coupling to enhance CO2 electrocatalytic activity by Mg-doping in Sr2FeMoO6-δ double perovskite for high performance solid oxide electrolysis cells. Nano Energy, 2021, 82, 105707.	16.0	67
34	CO2-emission-free electrocatalytic CH3OH selective upgrading with high productivity at large current densities for energy saved hydrogen co-generation. Nano Energy, 2021, 80, 105530.	16.0	76
35	Corrosion performance of candidate boiler tube alloys under advanced pressurized oxy-fuel combustion conditions. Energy, 2021, 215, 119178.	8.8	8
36	Condensed phase corrosion of P91 and DSS 2205 steels at advanced oxygenâ€fired pressurized fluidized bed combustion plants. Materials and Corrosion - Werkstoffe Und Korrosion, 2021, 72, 757-771.	1.5	3

#	Article	IF	CITATIONS
37	Co- and N-doped carbon nanotubes with hierarchical pores derived from metal–organic nanotubes for oxygen reduction reaction. Journal of Energy Chemistry, 2021, 53, 49-55.	12.9	18
38	Effect of interaction between two single-particle-impingements on the repassivation behavior of 304 stainless steel in a simulated groundwater. Corrosion Reviews, 2021, 39, 149-164.	2.0	1
39	Folic acid self-assembly synthesis of ultrathin N-doped carbon nanosheets with single-atom metal catalysts. Energy Storage Materials, 2021, 36, 409-416.	18.0	39
40	Characterizing foulants on slotted liner and probing the surface interaction mechanisms in organic media with implication for an antifouling strategy in oil production. Fuel, 2021, 290, 120008.	6.4	7
41	Folic Acid Self-Assembly Enabling Manganese Single-Atom Electrocatalyst for Selective Nitrogen Reduction to Ammonia. Nano-Micro Letters, 2021, 13, 125.	27.0	39
42	Corrosion of SS310 and Alloy 740 in high temperature supercritical CO2 with impurities H2O and O2. Corrosion Science, 2021, 184, 109350.	6.6	21
43	Electronic Delocalization of Bismuth Oxide Induced by Sulfur Doping for Efficient CO ₂ Electroreduction to Formate. ACS Catalysis, 2021, 11, 7604-7612.	11.2	80
44	High-Temperature Electrochemical Devices Based on Dense Ceramic Membranes for CO2 Conversion and Utilization. Electrochemical Energy Reviews, 2021, 4, 518-544.	25.5	27
45	Combating marine corrosion on engineered oxide surface by repelling, blocking and capturing Clâ^': A mini review. Corrosion Communications, 2021, 2, 1-7.	6.0	38
46	Role of Ca2+ in the CO2 corrosion behavior and film characteristics of N80 steel and electroless Ni–P coating at high temperature and high pressure. Materials Chemistry and Physics, 2021, 267, 124618.	4.0	12
47	Understanding the Roles of Electrogenerated Co ³⁺ and Co ⁴⁺ in Selectivityâ€Tuned 5â€Hydroxymethylfurfural Oxidation. Angewandte Chemie, 2021, 133, 20698-20705.	2.0	25
48	Understanding the Roles of Electrogenerated Co ³⁺ and Co ⁴⁺ in Selectivity‶uned 5â€Hydroxymethylfurfural Oxidation. Angewandte Chemie - International Edition, 2021, 60, 20535-20542.	13.8	121
49	Influence of H2S on the general corrosion and sulfide stress cracking of pipelines steels for supercritical CO2 transportation. Corrosion Science, 2021, 190, 109639.	6.6	20
50	Microfabrication of the Ammonia Plasma-Activated Nickel Nitride–Nickel Thin Film for Overall Water Splitting in the Microfluidic Membraneless Electrolyzer. ACS Applied Energy Materials, 2021, 4, 9639-9652.	5.1	18
51	Constructing proton transport channels in low phosphoric-acid doped polybenzimidazole membrane by introducing metal–organic frameworks containing phosphoric-acid groups. Journal of Power Sources, 2021, 507, 230316.	7.8	31
52	Energyâ€saving H ₂ Generation Coupled with Oxidative Alcohol Refining over Bimetallic Phosphide Ni ₂ Pâ^'CoP Junction Bifunctional Electrocatalysts. ChemSusChem, 2021, 14, 5450-5459.	6.8	16
53	La0.5Sr0.5Fe0.9Mo0.1O3-δ-CeO2 anode catalyst for Co-Producing electricity and ethylene from ethane in proton-conducting solid oxide fuel cells. Ceramics International, 2021, 47, 24106-24114.	4.8	39
54	Core–Shell Structured Cu(OH) ₂ @NiFe(OH) _{<i>x</i>} Nanotube Electrocatalysts for Methanol Oxidation Based Hydrogen Evolution. ACS Applied Nano Materials, 2021, 4, 8723-8732.	5.0	14

#	Article	IF	CITATIONS
55	Hierarchically assembling cobalt/nickel carbonate hydroxide on copper nitride nanowires for highly efficient water splitting. Applied Catalysis B: Environmental, 2021, 292, 120148.	20.2	62
56	In-situ exsolved FeNi nanoparticles on perovskite matrix anode for co-production of ethylene and power from ethane in proton conducting fuel cells. Electrochimica Acta, 2021, 393, 139096.	5.2	17
57	Rational design of CdCO3 nanoparticles decorated carbon nanofibers for boosting electrochemical CO2 reduction. Journal of Power Sources, 2021, 510, 230433.	7.8	10
58	Accelerating photoelectric CO2 conversion with a photothermal wavelength-dependent plasmonic local field. Applied Catalysis B: Environmental, 2021, 298, 120533.	20.2	17
59	Constructing stable continuous proton transport channels by in-situ preparation of covalent triazine-based frameworks in phosphoric acid-doped polybenzimidazole for high-temperature proton exchange membranes. Journal of Membrane Science, 2021, 640, 119775.	8.2	51
60	Bifunctional Pt–Co ₃ O ₄ electrocatalysts for simultaneous generation of hydrogen and formate <i>via</i> energy-saving alkaline seawater/methanol co-electrolysis. Journal of Materials Chemistry A, 2021, 9, 6316-6324.	10.3	65
61	Bi ₂ O ₃ Nanosheets Grown on Carbon Nanofiber with Inherent Hydrophobicity for High-Performance CO ₂ Electroreduction in a Wide Potential Window. ACS Nano, 2021, 15, 17757-17768.	14.6	47
62	Emerging anode materials architectured with NiCoFe ternary alloy nanoparticles for ethane-fueled protonic ceramic fuel cells. Journal of Power Sources, 2021, 515, 230634.	7.8	9
63	UnravelingÂthe Enhanced Kinetics of Sr ₂ Fe ₁₊ <i>_x</i> Mo _{1â€} <i>_x</i> Bectrocatalysts for Highâ€Performance Solid Oxide Cells. Advanced Energy Materials, 2021, 11, 2102845.	u b9. 5	41
64	Phosphoric acid-doped polybenzimidazole with a leaf-like three-layer porous structure as a high-temperature proton exchange membrane for fuel cells. Journal of Materials Chemistry A, 2021, 9, 26345-26353.	10.3	50
65	Hierarchically Assembling Cobalt/Nickel Carbonate Hydroxide on Copper Nitride Nanowires for Highly Efficient Water Splitting. ECS Meeting Abstracts, 2021, MA2021-02, 1734-1734.	0.0	0
66	Electronic Regulation of Bismuth Oxide Via Sulfur Doping for Efficient CO2 Electroreduction to Formate. ECS Meeting Abstracts, 2021, MA2021-02, 824-824.	0.0	0
67	Steering the Selectivity of CuO to Near-Unity of CO with Indium Species for CO2 Electroreduction. ECS Meeting Abstracts, 2021, MA2021-02, 825-825.	0.0	0
68	Electrochemically Dismantled Perovskite with Cooperative Catalysis for CO2-to-Formate Conversion. ECS Meeting Abstracts, 2021, MA2021-02, 1318-1318.	0.0	0
69	Enhanced CO2 Adsorption Capability for Highly Selective Electroreduction of CO2 to Formate. ECS Meeting Abstracts, 2021, MA2021-02, 1740-1740.	0.0	0
70	Coupling efficient biomass upgrading with H ₂ production <i>via</i> bifunctional Cu _x S@NiCo-LDH core–shell nanoarray electrocatalysts. Journal of Materials Chemistry A, 2020, 8, 1138-1146.	10.3	132
71	Wavy SnO2 catalyzed simultaneous reinforcement of carbon dioxide adsorption and activation towards electrochemical conversion of CO2 to HCOOH. Applied Catalysis B: Environmental, 2020, 261, 118243.	20.2	97
72	Stability of C3-C6 carbonium ions inside zeolites: A first principles study. Applied Surface Science, 2020, 503, 144148.	6.1	7

#	Article	IF	CITATIONS
73	A-site deficient perovskite with nano-socketed Ni-Fe alloy particles as highly active and durable catalyst for high-temperature CO2 electrolysis. Electrochimica Acta, 2020, 335, 135683.	5.2	38
74	Pr ₂ BaNiMnO _{7â^îr} double-layered Ruddlesden–Popper perovskite oxides as efficient cathode electrocatalysts for low temperature proton conducting solid oxide fuel cells. Journal of Materials Chemistry A, 2020, 8, 7704-7712.	10.3	84
75	Insights into the erosion-enhanced corrosion on electroless Ni–P coating from single particle impingement. Corrosion Science, 2020, 166, 108422.	6.6	22
76	Valueâ€Added Formate Production from Selective Methanol Oxidation as Anodic Reaction to Enhance Electrochemical Hydrogen Cogeneration. ChemSusChem, 2020, 13, 914-921.	6.8	87
77	CO2 dry reforming of CH4 with Sr and Ni co-doped LaCrO3 perovskite catalysts. Applied Surface Science, 2020, 506, 144699.	6.1	57
78	Unlocking the impurity-induced pipeline corrosion based on phase behavior of impure CO2 streams. Corrosion Science, 2020, 165, 108367.	6.6	19
79	Enhancing through-plane electrical conductivity by introducing Au microdots onto TiN coated metal bipolar plates of PEMFCs. International Journal of Hydrogen Energy, 2020, 45, 29442-29448.	7.1	31
80	Characterization and corrosion behavior of electroless Ni-Mo-P/Ni-P composite coating in CO2/H2S/Clâ^' brine: Effects of Mo addition and heat treatment. Surface and Coatings Technology, 2020, 403, 126416.	4.8	23
81	Unraveling Structure Sensitivity in CO ₂ Electroreduction to Near-Unity CO on Silver Nanocubes. ACS Catalysis, 2020, 10, 3158-3163.	11.2	80
82	Constructing multifunctional â€~Nanoplatelet-on-Nanoarray' electrocatalyst with unprecedented activity towards novel selective organic oxidation reactions to boost hydrogen production. Applied Catalysis B: Environmental, 2020, 278, 119339.	20.2	93
83	Electrolysis of waste water containing aniline to produce polyaniline and hydrogen with low energy consumption. International Journal of Hydrogen Energy, 2020, 45, 22419-22426.	7.1	21
84	Multi-functionalities enabled fivefold applications of LaCo0.6Ni0.4O3â^î´ in intermediate temperature symmetrical solid oxide fuel/electrolysis cells. Nano Energy, 2020, 77, 105207.	16.0	37
85	Recent Advances in MOFâ€Derived Single Atom Catalysts for Electrochemical Applications. Advanced Energy Materials, 2020, 10, 2001561.	19.5	265
86	"Revitalizing―degraded solid oxide fuel cells in sour fuels for bifunctional oxygen catalysis in zinc–air batteries. Green Chemistry, 2020, 22, 6075-6083.	9.0	9
87	Cogeneration of ethylene and electricity in symmetrical protonic solid oxide fuel cells based on a La _{0.6} Sr _{0.4} Fe _{0.8} Nb _{0.1} Cu _{0.1} O _{3â^îr} electrode. Journal of Materials Chemistry A, 2020, 8, 25978-25985.	10.3	22
88	A High-Performance Ruddlesden–Popper Perovskite for Bifunctional Oxygen Electrocatalysis. ACS Catalysis, 2020, 10, 13437-13444.	11.2	39
89	Oxygen Evolution Reaction: Core–Shell Structured NiFeSn@NiFe (Oxy)Hydroxide Nanospheres from an Electrochemical Strategy for Electrocatalytic Oxygen Evolution Reaction (Adv. Sci. 10/2020). Advanced Science, 2020, 7, 2070052.	11.2	13
90	<i>In Situ</i> Exsolved Metal Nanoparticles: A Smart Approach for Optimization of Catalysts. Chemistry of Materials, 2020, 32, 5424-5441.	6.7	89

#	Article	IF	CITATIONS
91	Hexagonal Zn Nanoplates Enclosed by Zn(100) and Zn(002) Facets for Highly Selective CO ₂ Electroreduction to CO. ACS Applied Materials & Interfaces, 2020, 12, 31431-31438.	8.0	51
92	Tuning adsorption strength of CO2 and its intermediates on tin oxide-based electrocatalyst for efficient CO2 reduction towards carbonaceous products. Applied Catalysis B: Environmental, 2020, 277, 119252.	20.2	50
93	Generating C4 Alkenes in Solid Oxide Fuel Cells via Cofeeding H ₂ and <i>n</i> -Butane Using a Selective Anode Electrocatalyst. ACS Applied Materials & Interfaces, 2020, 12, 16209-16215.	8.0	15
94	Understanding the immobilization mechanisms of hazardous heavy metal ions in the cage of sodalite at molecular level: A DFT study. Microporous and Mesoporous Materials, 2020, 306, 110409.	4.4	13
95	Standalone Solar Carbon-Based Fuel Production Based on Semiconductors. Cell Reports Physical Science, 2020, 1, 100101.	5.6	18
96	Corrosion of duplex stainless steel 2205 in hot flue gas environments produced at advanced oxy-fired pressurized fluidized bed combustion plants. International Journal of Greenhouse Gas Control, 2020, 100, 103108.	4.6	3
97	Amorphous cobalt hydroxysulfide nanosheets with regulated electronic structure for high-performance electrochemical energy storage. Science China Materials, 2020, 63, 2303-2313.	6.3	13
98	Metal-support interaction enhanced electrochemical reduction of CO2 to formate between graphene and Bi nanoparticles. Journal of CO2 Utilization, 2020, 37, 353-359.	6.8	41
99	Ca-containing Ba0·95Ca0·05Co0·4Fe0·4Zr0·1Y0·1O3-δ cathode with high CO2-poisoning tolerance for proton-conducting solid oxide fuel cells. Journal of Power Sources, 2020, 453, 227909.	7.8	35
100	Surface Interactions between Water-in-Oil Emulsions with Asphaltenes and Electroless Nickel–Phosphorus Coating. Langmuir, 2020, 36, 897-905.	3.5	12
101	Novel folic acid complex derived nitrogen and nickel co-doped carbon nanotubes with embedded Ni nanoparticles as efficient electrocatalysts for CO ₂ reduction. Journal of Materials Chemistry A, 2020, 8, 5105-5114.	10.3	18
102	Boosting H ₂ Generation Coupled with Selective Oxidation of Methanol into Valueâ€Added Chemical over Cobalt Hydroxide@Hydroxysulfide Nanosheets Electrocatalysts. Advanced Functional Materials, 2020, 30, 1909610.	14.9	190
103	Exploring Ni(Mn _{1/3} Cr _{2/3}) ₂ O ₄ spinel-based electrodes for solid oxide cells. Journal of Materials Chemistry A, 2020, 8, 3988-3998.	10.3	27
104	Review—Electrochemical Noise Applied in Corrosion Science: Theoretical and Mathematical Models towards Quantitative Analysis. Journal of the Electrochemical Society, 2020, 167, 081507.	2.9	78
105	γ-MnO2 nanorod-assembled hierarchical micro-spheres with oxygen vacancies to enhance electrocatalytic performance toward the oxygen reduction reaction for aluminum-air batteries. Journal of Energy Chemistry, 2020, 51, 81-89.	12.9	45
106	Co P@NiCo-LDH heteronanosheet arrays as efficient bifunctional electrocatalysts for co-generation of value-added formate and hydrogen with less-energy consumption. Journal of Energy Chemistry, 2020, 50, 314-323.	12.9	83
107	In situ embedding of CoFe nanocatalysts into Sr3FeMoO7 matrix as high-performance anode materials for solid oxide fuel cells. Journal of Power Sources, 2020, 459, 228071.	7.8	31
108	Boosting formate production at high current density from CO2 electroreduction on defect-rich hierarchical mesoporous Bi/Bi2O3 junction nanosheets. Applied Catalysis B: Environmental, 2020, 271, 118957.	20.2	103

#	Article	IF	CITATIONS
109	Tuning local carbon active sites saturability of graphitic carbon nitride to boost CO2 electroreduction towards CH4. Nano Energy, 2020, 73, 104833.	16.0	35
110	Perovskite Chromite With In-Situ Assembled Ni-Co Nano-Alloys: A Potential Bifunctional Electrode Catalyst for Solid Oxide Cells. Frontiers in Chemistry, 2020, 8, 595608.	3.6	7
111	Insights into the Electrochemical Corrosion Behavior and Mechanism of Electroless Ni-P Coating in the CO2/H2S/Clâ [~] ' Environment. Corrosion, 2020, 76, 578-590.	1.1	18
112	Shape Effect of Zinc Nanostructures on Electrochemical CO ₂ Reduction. ECS Meeting Abstracts, 2020, MA2020-02, 3877-3877.	0.0	1
113	Investigation on the flow-induced corrosion and degradation behavior of underground J55 pipe in a water production well in the Athabasca oil sands reservoir. Journal of Petroleum Science and Engineering, 2019, 182, 106325.	4.2	23
114	Electrochemical Transformation of Facetâ€Controlled BiOI into Mesoporous Bismuth Nanosheets for Selective Electrocatalytic Reduction of CO ₂ to Formic Acid. ChemSusChem, 2019, 12, 4700-4707.	6.8	46
115	Hollow Porous Ag Spherical Catalysts for Highly Efficient and Selective Electrocatalytic Reduction of CO ₂ to CO. ACS Sustainable Chemistry and Engineering, 2019, 7, 14443-14450.	6.7	40
116	Modeling the effect of insoluble corrosion products on pitting corrosion kinetics of metals. Npj Materials Degradation, 2019, 3, .	5.8	46
117	Minimum and well-dispersed platinum nanoparticles on 3D porous nickel for highly efficient electrocatalytic hydrogen evolution reaction enabled by atomic layer deposition. Applied Surface Science, 2019, 494, 1091-1099.	6.1	20
118	Electrolyte Driven Highly Selective CO ₂ Electroreduction at Low Overpotentials. ACS Catalysis, 2019, 9, 10440-10447.	11.2	41
119	Exploring MnCr2O4–Gd0.1Ce0.9O2-î´ as a composite electrode material for solid oxide fuel cell. International Journal of Hydrogen Energy, 2019, 44, 31333-31341.	7.1	16
120	Anion Vacancies Regulating Endows MoSSe with Fast and Stable Potassium Ion Storage. ACS Nano, 2019, 13, 11843-11852.	14.6	210
121	Review—Factors Influencing Sulfur Induced Corrosion on the Secondary Side in Pressurized Water Reactors (PWRs). Journal of the Electrochemical Society, 2019, 166, C49-C64.	2.9	42
122	Sulfur induced corrosion (SIC) mechanism of steam generator (SG) tubing at micro scale: A critical review. Materials Chemistry and Physics, 2019, 233, 133-140.	4.0	36
123	Transient Potential Induced Anodic Dissolution of 316L Stainless Steel in Sulfuric Acid Solution. Journal of the Electrochemical Society, 2019, 166, C3355-C3363.	2.9	8
124	Investigation of the Antifouling Mechanism of Electroless Nickel–Phosphorus Coating against Sand and Bitumen. Energy & Fuels, 2019, 33, 6350-6360.	5.1	2
125	Achieving Efficient CO ₂ Electrochemical Reduction on Tunable In(OH) ₃ -Coupled Cu ₂ O-Derived Hybrid Catalysts. ACS Applied Materials & Interfaces, 2019, 11, 22346-22351.	8.0	28
126	Effects of reduced sulfur on passive film properties of steam generator (SG) tubing: an overview. Anti-Corrosion Methods and Materials, 2019, 66, 317-326.	1.5	7

#	Article	IF	CITATIONS
127	Gum Arabic as corrosion inhibitor in the oil industry: experimental and theoretical studies. Corrosion Engineering Science and Technology, 2019, 54, 444-454.	1.4	39
128	Fouling mechanisms of asphaltenes and fine solids on bare and electroless nickel-phosphorus coated carbon steel. Fuel, 2019, 252, 188-199.	6.4	11
129	Microwave-assisted hydrothermal synthesis of MOFs-derived bimetallic CuCo-N/C electrocatalyst for efficient oxygen reduction reaction. Journal of Alloys and Compounds, 2019, 795, 462-470.	5.5	31
130	Insights into the Interfacial Process in Electroless Ni–P Coating on Supercritical CO ₂ Transport Pipeline as Relevant to Carbon Capture and Storage. ACS Applied Materials & Interfaces, 2019, 11, 16243-16251.	8.0	27
131	Electrochemical exfoliation from an industrial ingot: ultrathin metallic bismuth nanosheets for excellent CO ₂ capture and electrocatalytic conversion. Nanoscale, 2019, 11, 22125-22133.	5.6	34
132	<i>In situ</i> grown cobalt phosphide (CoP) on perovskite nanofibers as an optimized trifunctional electrocatalyst for Zn–air batteries and overall water splitting. Journal of Materials Chemistry A, 2019, 7, 26607-26617.	10.3	92
133	Carbon nanofibers@NiSe core/sheath nanostructures as efficient electrocatalysts for integrating highly selective methanol conversion and less-energy intensive hydrogen production. Journal of Materials Chemistry A, 2019, 7, 25878-25886.	10.3	57
134	Unraveling the effects of CO2 and H2S on the corrosion behavior of electroless Ni-P coating in CO2/H2S/Cl– environments at high temperature and high pressure. Corrosion Science, 2019, 148, 317-330.	6.6	63
135	Sensing corrosion within an artificial defect in organic coating using SECM. Sensors and Actuators B: Chemical, 2019, 280, 235-242.	7.8	41
136	Probing the Interaction Mechanism between Oil-in-Water Emulsions and Electroless Nickel–Phosphorus Coating with Implications for Antifouling in Oil Production. Energy & Fuels, 2019, 33, 3764-3775.	5.1	11
137	Effects of hydrogen and stress on the electrochemical and passivation behaviour of 304 stainless steel in simulated PEMFC environment. Electrochimica Acta, 2019, 293, 60-77.	5.2	68
138	Co ₂ CrO ₄ Nanopowders as an Anode Catalyst for Simultaneous Conversion of Ethane to Ethylene and Power in Proton-Conducting Fuel Cell Reactors. Journal of Physical Chemistry C, 2018, 122, 4165-4171.	3.1	23
139	A facile surface chemistry approach to bifunctional excellence for perovskite electrocatalysis. Nano Energy, 2018, 49, 117-125.	16.0	55
140	Characterization of microstructure and properties of electroless duplex Ni-W-P/Ni-P nano-ZrO2 composite coating. Materials Today Physics, 2018, 4, 36-42.	6.0	37
141	Effect of defect on corrosion behavior of electroless Ni-P coating in CO2-saturated NaCl solution. Corrosion Science, 2018, 134, 23-37.	6.6	57
142	Rational Design of Silver Sulfide Nanowires for Efficient CO ₂ Electroreduction in Ionic Liquid. ACS Catalysis, 2018, 8, 1469-1475.	11.2	76
143	Toward a rational photocatalyst design: a new formation strategy of co-catalyst/semiconductor heterostructures <i>via in situ</i> exsolution. Chemical Communications, 2018, 54, 1505-1508.	4.1	39
144	Ultrathin 5-fold twinned sub-25 nm silver nanowires enable highly selective electroreduction of CO2 to CO. Nano Energy, 2018, 45, 456-462.	16.0	115

#	Article	IF	CITATIONS
145	Descriptor of catalytic activity of metal sulfides for oxygen reduction reaction: a potential indicator for mineral flotation. Journal of Materials Chemistry A, 2018, 6, 9650-9656.	10.3	41
146	Facile Preparation of Self-Standing Hierarchical Porous Nitrogen-Doped Carbon Fibers for Supercapacitors from Plant Protein–Lignin Electrospun Fibers. ACS Omega, 2018, 3, 4647-4656.	3.5	38
147	Cogeneration of ethylene and energy in protonic fuel cell with an efficient and stable anode anchored with in-situ exsolved functional metal nanoparticles. Applied Catalysis B: Environmental, 2018, 220, 283-289.	20.2	60
148	Zr ₂ N ₂ O Coating-Improved Corrosion Resistance for the Anodic Dissolution Induced by Cathodic Transient Potential. ACS Applied Materials & Interfaces, 2018, 10, 40111-40124.	8.0	19
149	Multiple-doped barium cerate proton-conducting electrolytes for chemical-energy cogeneration in solid oxide fuel cells. International Journal of Hydrogen Energy, 2018, 43, 19704-19710.	7.1	14
150	Activating p-Blocking Centers in Perovskite for Efficient Water Splitting. CheM, 2018, 4, 2902-2916.	11.7	99
151	A strongly cooperative spinel nanohybrid as an efficient bifunctional oxygen electrocatalyst for oxygen reduction reaction and oxygen evolution reaction. Applied Catalysis B: Environmental, 2018, 236, 413-419.	20.2	82
152	Achieving ultrahigh corrosion resistance and conductive zirconium oxynitride coating on metal bipolar plates by plasma enhanced atomic layer deposition. Journal of Power Sources, 2018, 397, 32-36.	7.8	37
153	Phase-field model of pitting corrosion kinetics in metallic materials. Npj Computational Materials, 2018, 4, .	8.7	49
154	High Performance Tubular Solid Oxide Fuel Cell Based on Ba _{0.5} Sr _{0.5} Ce _{0.6} Zr _{0.2} Gd _{0.1} Y _{0.1} Conducting Electrolyte. Journal of the Electrochemical Society, 2018, 165, F764-F769.	C <audo>3-ĺ</audo>	Proto
155	Thermally stable and coking resistant CoMo alloy-based catalysts as fuel electrodes for solid oxide electrochemical cells. Journal of Materials Chemistry A, 2018, 6, 15377-15385.	10.3	21
156	The surface evolution of La0.4Sr0.6TiO3+δanode in solid oxide fuel cells: Understanding the sulfur-promotion effect. Journal of Power Sources, 2017, 343, 127-134.	7.8	14
157	Shape-Dependent Electrocatalytic Reduction of CO ₂ to CO on Triangular Silver Nanoplates. Journal of the American Chemical Society, 2017, 139, 2160-2163.	13.7	551
158	A rational design for enhanced oxygen reduction: Strongly coupled silver nanoparticles and engineered perovskite nanofibers. Nano Energy, 2017, 38, 392-400.	16.0	60
159	Au/CeO ₂ hollow nanospheres with enhanced catalytic activity for <scp>CO</scp> oxidation. International Journal of Applied Ceramic Technology, 2017, 14, 908-914.	2.1	4
160	Developing hierarchically porous MnO _x /NC hybrid nanorods for oxygen reduction and evolution catalysis. Green Chemistry, 2017, 19, 2793-2797.	9.0	57
161	The excellence of La(Sr)Fe(Ni)O ₃ as an active and efficient cathode for direct CO ₂ electrochemical reduction at elevated temperatures. Journal of Materials Chemistry A, 2017, 5, 2673-2680.	10.3	78
162	A coupling for success: Controlled growth of Co/CoOx nanoshoots on perovskite mesoporous nanofibres as high-performance trifunctional electrocatalysts in alkaline condition. Nano Energy, 2017, 32, 247-254.	16.0	189

#	Article	IF	CITATIONS
163	Fabrication and characterization of a tubular ceramic fuel cell based on BaZr0.1Ce0.7Y0.1Yb0.1O3-δ proton conducting electrolyte. Journal of Power Sources, 2017, 341, 264-269.	7.8	42
164	Allâ€Inâ€One Perovskite Catalyst: Smart Controls of Architecture and Composition toward Enhanced Oxygen/Hydrogen Evolution Reactions. Advanced Energy Materials, 2017, 7, 1700666.	19.5	124
165	Enhancing Perovskite Electrocatalysis of Solid Oxide Cells Through Controlled Exsolution of Nanoparticles. ChemSusChem, 2017, 10, 3333-3341.	6.8	97
166	Alternative Fuel Cell Technologies for Cogenerating Electrical Power and Syngas from Greenhouse Gases. ACS Energy Letters, 2017, 2, 1789-1796.	17.4	37
167	Stabilizing Double Perovskite for Effective Bifunctional Oxygen Electrocatalysis in Alkaline Conditions. Chemistry of Materials, 2017, 29, 6228-6237.	6.7	94
168	Grafting doped manganite into nickel anode enables efficient and durable energy conversions in biogas solid oxide fuel cells. Applied Catalysis B: Environmental, 2017, 200, 174-181.	20.2	27
169	Corrosion Mechanisms and Materials Selection for the Construction of Flue Gas Component in Advanced Heat and Power Systems. Industrial & Engineering Chemistry Research, 2017, 56, 14141-14154.	3.7	24
170	Passivation degradation of Alloy 800 on nucleate boiling surface. Corrosion Engineering Science and Technology, 2017, 52, 391-396.	1.4	1
171	Hydrogen-enhanced Surface Reactivity of X80 Pipeline Steel observed by Scanning Electrochemical Microscopy. Electrochemistry, 2016, 84, 238-242.	1.4	10
172	Highly Active and Redox-Stable Ce-Doped LaSrCrFeO-Based Cathode Catalyst for CO ₂ SOECs. ACS Applied Materials & Interfaces, 2016, 8, 6457-6463.	8.0	101
173	Enhancing Sulfur Tolerance of Ni-Based Cermet Anodes of Solid Oxide Fuel Cells by Ytterbium-Doped Barium Cerate Infiltration. ACS Applied Materials & Interfaces, 2016, 8, 10293-10301.	8.0	54
174	Lead-induced stress corrosion cracking behavior of mechanically surface-treated alloy 690. Materials Research Letters, 2016, 4, 180-184.	8.7	5
175	The evolution of hierarchical porosity in self-templated nitrogen-doped carbons and its effect on oxygen reduction electrocatalysis. RSC Advances, 2016, 6, 80398-80407.	3.6	46
176	Solid-Liquid Mass Transfer under Flow Boiling Condition. Journal of the Electrochemical Society, 2016, 163, H618-H624.	2.9	2
177	Highly Stable and Efficient Catalyst with In Situ Exsolved Fe–Ni Alloy Nanospheres Socketed on an Oxygen Deficient Perovskite for Direct CO ₂ Electrolysis. ACS Catalysis, 2016, 6, 6219-6228.	11.2	206
178	New Opportunity for <i>in Situ</i> Exsolution of Metallic Nanoparticles on Perovskite Parent. Nano Letters, 2016, 16, 5303-5309.	9.1	222
179	Anodeâ€Engineered Protonic Ceramic Fuel Cell with Excellent Performance and Fuel Compatibility. Advanced Materials, 2016, 28, 8922-8926.	21.0	94
180	Smart utilization of cobaltite-based double perovskite cathodes on barrier-layer-free zirconia electrolyte of solid oxide fuel cells. Journal of Materials Chemistry A, 2016, 4, 19019-19025.	10.3	51

#	Article	IF	CITATIONS
181	CO ₂ -to-CO conversion on layered perovskite with in situ exsolved Co–Fe alloy nanoparticles: an active and stable cathode for solid oxide electrolysis cells. Journal of Materials Chemistry A, 2016, 4, 17521-17528.	10.3	106
182	Fuel Cells: Anodeâ€Engineered Protonic Ceramic Fuel Cell with Excellent Performance and Fuel Compatibility (Adv. Mater. 40/2016). Advanced Materials, 2016, 28, 8921-8921.	21.0	1
183	A bifunctional solid oxide electrolysis cell for simultaneous CO ₂ utilization and synthesis gas production. Chemical Communications, 2016, 52, 13687-13690.	4.1	10
184	The Excellence of Both Worlds: Developing Effective Double Perovskite Oxide Catalyst of Oxygen Reduction Reaction for Room and Elevated Temperature Applications. Advanced Functional Materials, 2016, 26, 4106-4112.	14.9	106
185	Facile Synthesis of Highly Active and Robust Ni–Mo Bimetallic Electrocatalyst for Hydrocarbon Oxidation in Solid Oxide Fuel Cells. ACS Energy Letters, 2016, 1, 225-230.	17.4	27
186	Developing a Thermal- and Coking-Resistant Cobalt–Tungsten Bimetallic Anode Catalyst for Solid Oxide Fuel Cells. ACS Catalysis, 2016, 6, 4630-4634.	11.2	26
187	Toward highly efficient in situ dry reforming of H ₂ S contaminated methane in solid oxide fuel cells via incorporating a coke/sulfur resistant bimetallic catalyst layer. Journal of Materials Chemistry A, 2016, 4, 9080-9087.	10.3	26
188	Bifunctional Catalyst of Core–Shell Nanoparticles Socketed on Oxygen-Deficient Layered Perovskite for Soot Combustion: <i>In Situ</i> Observation of Synergistic Dual Active Sites. ACS Catalysis, 2016, 6, 2710-2714.	11.2	70
189	A study on corrosion behaviors of Ni–Cr–Mo laser coating, 316 stainless steel and X70 steel in simulated solutions with H2S and CO2. Surface and Coatings Technology, 2016, 291, 250-257.	4.8	57
190	Biogas to syngas: flexible on-cell micro-reformer and NiSn bimetallic nanoparticle implanted solid oxide fuel cells for efficient energy conversion. Journal of Materials Chemistry A, 2016, 4, 4603-4609.	10.3	30
191	Double-Layered Perovskite Anode with <i>in Situ</i> Exsolution of a Co–Fe Alloy To Cogenerate Ethylene and Electricity in a Proton-Conducting Ethane Fuel Cell. ACS Catalysis, 2016, 6, 760-768.	11.2	95
192	Carbon-resistant Ni-Zr0.92Y0.08O2-δ supported solid oxide fuel cells using Ni-Cu-Fe alloy cermet as on-cell reforming catalyst and mixed methane-steam as fuel. Journal of Power Sources, 2016, 303, 340-346.	7.8	30
193	Novel layered solid oxide fuel cells with multiple-twinned Ni _{0.8} Co _{0.2} nanoparticles: the key to thermally independent CO ₂ utilization and power-chemical cogeneration. Energy and Environmental Science, 2016, 9, 207-215.	30.8	103
194	Passivity degradation of alloy 800 in simulated crevice chemistries. Transactions of Tianjin University, 2015, 21, 234-243.	6.4	18
195	Monitoring the Diffusion Layer During Passive Film Breakdown on Alloy 800 with Digital Holography. Acta Metallurgica Sinica (English Letters), 2015, 28, 1170-1174.	2.9	7
196	A-site-deficiency facilitated in situ growth of bimetallic Ni–Fe nano-alloys: a novel coking-tolerant fuel cell anode catalyst. Nanoscale, 2015, 7, 11173-11181.	5.6	107
197	A-site deficient perovskite: the parent for in situ exsolution of highly active, regenerable nano-particles as SOFC anodes. Journal of Materials Chemistry A, 2015, 3, 11048-11056.	10.3	164
198	A-site deficient chromite perovskite with in situ exsolution of nano-Fe: a promising bi-functional catalyst bridging the growth of CNTs and SOFCs. Journal of Materials Chemistry A, 2015, 3, 14625-14630.	10.3	49

#	Article	IF	CITATIONS
199	Highly cost-effective and sulfur/coking resistant VO _x -grafted TiO ₂ nanoparticles as an efficient anode catalyst for direct conversion of dry sour methane in solid oxide fuel cells. Journal of Materials Chemistry A, 2015, 3, 23973-23980.	10.3	14
200	Semiconductivity Conversion of Passive Films on Alloy 800 in Chloride Solutions Containing Various Concentrations of Thiosulfate. Journal of the Electrochemical Society, 2015, 162, C482-C486.	2.9	21
201	Development of electroless Ni–P/nano-WC composite coatings and investigation on its properties. Surface and Coatings Technology, 2015, 277, 99-106.	4.8	115
202	A mechanistic study of sulfur-induced passivity degradation of Alloy 800 in a simulated alkaline crevice environment at 300 ŰC. Journal of Solid State Electrochemistry, 2015, 19, 3567-3578.	2.5	13
203	Understanding the interaction of thiosulfate with Alloy 800 in aqueous chloride solutions using SECM. Journal of Electroanalytical Chemistry, 2015, 744, 77-84.	3.8	31
204	Electrochemical oxidation of sour natural gas over La0.4Ce0.6O1.8–La0.4Sr0.6TiO3±δ anode in SOFC: A mechanism study of H2S effects. Applied Catalysis B: Environmental, 2015, 176-177, 627-636.	20.2	23
205	An ingenious Ni/Ce co-doped titanate based perovskite as a coking-tolerant anode material for direct hydrocarbon solid oxide fuel cells. Journal of Materials Chemistry A, 2015, 3, 22830-22838.	10.3	42
206	Carbon-tolerant Ni-based cermet anodes modified by proton conducting yttrium- and ytterbium-doped barium cerates for direct methane solid oxide fuel cells. Journal of Materials Chemistry A, 2015, 3, 21609-21617.	10.3	56
207	A mechanistic study on sulfur-induced passivity degradation on Alloy 800 in simulated alkaline crevice chemistries at temperatures ranging from 21 ŰC to 300 ŰC. Corrosion Science, 2015, 100, 504-516.	6.6	27
208	Promoting Influence of Doping Indium into BaCe _{0.5} Zr _{0.3} Y _{0.2} O _{3â€Î´} as Solid Proton Conductor. International Journal of Applied Ceramic Technology, 2015, 12, 1174-1183.	2.1	11
209	Nanotubular surface modification of metallic implants via electrochemical anodization technique. International Journal of Nanomedicine, 2014, 9, 4421.	6.7	43
210	Memory effect and recoverability of passive film degradation of Alloy 800 in simulated crevice chemistry. Nuclear Engineering and Design, 2014, 280, 57-61.	1.7	3
211	pH Effect on Sulfur-Induced Passivity Degradation of Alloy 800 in Simulated Crevice Chemistries. Journal of the Electrochemical Society, 2014, 161, C201-C214.	2.9	38
212	Co-generation of energy and ethylene in hydrocarbon fueled SOFCs with Cr3C2 and WC anode catalysts. Ceramics International, 2014, 40, 11781-11786.	4.8	10
213	Progress in La-doped SrTiO ₃ (LST)-based anode materials for solid oxide fuel cells. RSC Advances, 2014, 4, 118-131.	3.6	157
214	Semiconductivity conversion of Alloy 800 in sulphate, thiosulphate, and chloride solutions. Corrosion Science, 2014, 87, 265-277.	6.6	30
215	Improved coking resistance of direct ethanol solid oxide fuel cells with a Ni–Sx anode. Journal of Power Sources, 2014, 250, 212-219.	7.8	11
216	Silverâ€coated copper nanowires with improved antiâ€oxidation property as conductive fillers in Iowâ€density polyethylene. Canadian Journal of Chemical Engineering, 2013, 91, 630-637.	1.7	26

#	Article	IF	CITATIONS
217	Electrochemical behavior of CoCrMo implant in Ringer's solution. Surface and Interface Analysis, 2013, 45, 1323-1328.	1.8	11
218	Cobalt doped LaSrTiO3â^δas an anode catalyst: effect of Co nanoparticle precipitation on SOFCs operating on H2S-containing hydrogen. Journal of Materials Chemistry A, 2013, 1, 9689.	10.3	56
219	Preparation and characterization of an solid oxide fuel cell tubular cellÂfor direct use with sour gas. Journal of Power Sources, 2013, 240, 411-416.	7.8	11
220	A mechanistic study on thiosulfate-enhanced passivity degradation of Alloy 800 in chloride solutions. Electrochimica Acta, 2013, 111, 510-525.	5.2	81
221	Effect of substitution of B-sites by Mn, Fe and Co in double perovskite-type Ba3CaNb2O9 on structure and electrical properties. RSC Advances, 2013, 3, 23824.	3.6	16
222	Oxidation kinetics of copper nanowires synthesized by AC electrodeposition of copper into porous aluminum oxide templates. Journal of Materials Research, 2012, 27, 1755-1762.	2.6	8
223	An investigation of fuel composition and flowâ€rate effects in a H ₂ S fuelled sofc: Experiments and thermodynamic analysis. Canadian Journal of Chemical Engineering, 2012, 90, 1033-1042.	1.7	5
224	Pitting susceptibility of induction-quenched pipeline with microstructural heterogeneity. Journal of Materials Science, 2012, 47, 6823-6834.	3.7	10
225	CO2 emission free co-generation of energy and ethylene in hydrocarbon SOFC reactors with a dehydrogenation anode. Physical Chemistry Chemical Physics, 2011, 13, 19615.	2.8	14
226	Formation of Hydroxyapatite Coating on Anodic Titanium Dioxide Nanotubes via an Efficient Dipping Treatment. Metallurgical and Materials Transactions A: Physical Metallurgy and Materials Science, 2011, 42, 3255-3264.	2.2	9
227	Ethane dehydrogenation over nano-Cr2O3 anode catalyst in proton ceramic fuel cell reactors to co-produce ethylene and electricity. Journal of Power Sources, 2011, 196, 1036-1041.	7.8	49
228	Nanoparticles as Anode Catalyst for Ethane Proton Conducting Fuel Cell Reactors to Coproduce Ethylene and Electricity. Advances in Physical Chemistry, 2011, 2011, 1-6.	2.0	9
229	Near-Neutral pH Stress Corrosion Cracking Susceptibility of Plastically Prestrained X70 Steel Weldment. Metallurgical and Materials Transactions A: Physical Metallurgy and Materials Science, 2010, 41, 2538-2547.	2.2	17
230	Y-doped BaCeO3â ^{~1} δ nanopowders as proton-conducting electrolyte materials for ethane fuel cells to co-generate ethylene and electricity. Journal of Power Sources, 2010, 195, 2659-2663.	7.8	62
231	Fabrication of bi-layered proton conducting membrane for hydrocarbon solid oxide fuel cell reactors. Electrochimica Acta, 2010, 55, 1145-1149.	5.2	24
232	An integral proton conducting SOFC for simultaneous production of ethylene and power from ethane. Chemical Communications, 2010, 46, 2052.	4.1	31
233	Correlation of Fuel Cell Anode Electrocatalytic and ex situ Catalytic Activity of Perovskites La _{0.75} Sr _{0.25} Cr _{0.5} X _{0.5} O _{3â^î´} (X = Ti, Mn, Fe,)	[j &.7 Qq1]	0 <i>8</i> 84314
234	Sulfur-Tolerant Anode Catalyst for Solid Oxide Fuel Cells Operating on H2S-Containing Syngas. Chemistry of Materials, 2010, 22, 1032-1037.	6.7	40

#	Article	IF	CITATIONS
235	Guest editorial-fuel cells. Asia-Pacific Journal of Chemical Engineering, 2009, 4, 1-2.	1.5	0
236	1â€D dynamic modeling of SOFC with analytical solution for reacting gasâ€flow problem. AICHE Journal, 2008, 54, 1537-1553.	3.6	13
237	Protonic membrane for fuel cell for co-generation of power and ethylene. Journal of Power Sources, 2008, 176, 122-127.	7.8	31
238	LaCrO3â^'VOxâ^'YSZ Anode Catalyst for Solid Oxide Fuel Cell Using Impure Hydrogen. Journal of Physical Chemistry C, 2007, 111, 16679-16685.	3.1	18
239	Performance of Ethane/Oxygen Fuel Cells Using Yttrium-Doped Barium Cerate as Electrolyte at Intermediate Temperatures. Journal of Physical Chemistry C, 2007, 111, 5069-5074.	3.1	37
240	Fabrication and performance of PEN SOFCs with proton-conducting electrolyte. Frontiers of Chemical Engineering in China, 2007, 1, 40-44.	0.6	0
241	Corrosion and wear resistance of chrome white irons—A correlation to their composition and microstructure. Metallurgical and Materials Transactions A: Physical Metallurgy and Materials Science, 2006, 37, 3029-3038.	2.2	54
242	Nonlinear state space modeling and simulation of a SOFC fuel cell. , 2006, , .		6
243	Title is missing!. Journal of Materials Science Letters, 2002, 21, 1195-1198.	0.5	8